Journal of Power Sources 198 (2012) 170–175

Contents lists available at SciVerse ScienceDirect

Journal of Power Sources

journal homepage: www.elsevier.com/locate/jpowsour

Investigation on the durability of direct dimethyl ether fuel cell. Part I: Anode degradation

Le-Hong Xing, Ge-Ping Yin*, Zhen-Bo Wang, Sheng Zhang, Yun-Zhi Gao, Chun-Yu Du

State Key Laboratory of Urban Water Resource and Environment, School of Chemical Engineering and Technology, Harbin Institute of Technology, No. 92, West Da-Zhi Street, Harbin 150001, China

ARTICLE INFO

Article history:
Received 19 August 2011
Received in revised form
25 September 2011
Accepted 26 September 2011
Available online 1 October 2011

Keywords:
Direct dimethyl ether fuel cell
Durability test
Anode catalyst degradation
Electrochemical active surface
Dimethyl ether oxidation

ABSTRACT

In the present study, anode degradation of a direct dimethyl ether fuel cell (DDFC) has been investigated after a 70.5 h discontinuous galvostatic operation at 60 °C under ambient pressure. Cyclic voltammetry and electrochemical impedance spectroscopy show that the anode performance decreases after the durability test. Characterizations of XRD and TEM confirm the growth of Pt particles (from 3.0 nm to 5.5 nm) during durability test, which causes the loss of anode electrochemical active surface (EAS). Cyclic voltammetry reveals that poisoning of catalyst by absorbed DME oxidation intermediates species is another cause of anode degradation. And the dissolution of anode Pt is not observed through energy dispersive analysis of X-ray (EDAX) during the durability test. In a companion article (Part II), the effect of cathode degradation on the long-term performance of DDFC is investigated.

1. Introduction

Fuel cells have been widely studied due to their high energy efficiency, low exhaustion and simplicity in structure [1–4]. Dimethyl ether (DME) is regarded as a promising fuel for fuel cells [5,6]. DME is easy to store and transport in comparison with hydrogen, because the physical properties of DME are similar with liquefied petroleum gas (LPG) [7]. DME has many advantages in comparison with methanol in terms of high energy density, low toxicity and low energy loss due to crossover effect [8,9]. Therefore, DME is considered as a new proper fuel for direct type fuel cells and has recently been receiving increasing attention [10,11].

Up to now, most of the research has been focused upon electrooxidation of DME [12,13] and the short-term performance of direct dimethyl ether fuel cell (DDFC) [14–16]. The long-term performance and durability of the membrane electrode assembly (MEA) for DDFC have not been investigated in detail. The long-term performance of DDFC must be different from proton exchange membrane fuel cell (PEMFC) and direct methanol fuel cell (DMFC) due to the unique oxidation reaction mechanism and the different intermediates and products of DME. The fading of the MEA is associated with the degradation of catalyst [17], poisoning of catalyst by accumulated intermediates from DME electro-oxidation or impurities [18,19], the aging of the electrolyte membrane [20,21], and variations of the wettability properties and pore structures in the catalyst layers and diffusion layers [22,23]. Preliminary research results indicate that the electrocatalysts' stability plays an important role in the long-term operation of fuel cells [24–26]. As a key component of MEA, the stability of anode has gained more attention. Wang et al. [27] find experimentally that the degradation of anodic Pt–Ru catalyst in DMFC proceeds gradually, and its degree is time-dependent. The particle size of catalyst is observed to increase with time. The contents of Pt and Ru oxides in anode catalyst increase, and the metal contents decrease with operation time. Jeon et al. [28] reveal that the contribution of the cathode on DMFC performance decay is larger than that of the anode because the cathode operates in harsh corrosion conditions. However, Liu et al. [29] consider that the agglomeration of catalyst in anode is more serious than that in cathode, because methanol might be more aggressive towards the catalyst than water.

In this work, a 70.5 h durability test of DDFC is carried out at 60 °C using homemade 40 wt.% Pt/C catalyst. The 70.5 h operation is composed of a 40.5 h operation beginning, and then cyclic voltammetry (CV) scans of the anode and cathode respectively, and another 30 h operation. On the basis of physical and electrochemical test results, the deterioration of anode performance is analyzed. Anode degradation is mainly caused by the growth of Pt particles and the poisoning of catalyst.

* Corresponding author. Tel.: +86 451 86413707; fax: +86 451 86413720.
E-mail address: yingeping@hit.edu.cn (G.-P. Yin).

0378-7753/$ – see front matter © 2011 Elsevier B.V. All rights reserved.
doi:10.1016/j.jpowsour.2011.09.090

2. Experimental

2.1. MEA fabrication

The working area of the MEA was 5 cm^2 (2.25 cm×2.25 cm). The anode and cathode catalyst were both 40 wt.% Pt/C. The catalyst powder and 5 wt.% Nafion ionomer solution (DuPont) were ultrasonically mixed in isopropyl alcohol to form a homogeneous catalyst ink. The anode catalyst ink was prepared similarly with the cathode catalyst ink. Then the ink was scraped onto the diffusion layer. The Nafion content was 20 wt.% in catalyst layers. The Pt loading of anode and cathode was 3.2 mg cm^{-2} and 2.5 mg cm^{-2}, respectively. The anode diffusion layers were wet-proofed Toray carbon papers (18 wt.% PTFE). The cathode diffusion layers were wet-proofed Toray carbon papers (30 wt.% PTFE) coated with 1 mg cm^{-2} Vulcan XC-72 carbon blacks and 30 wt.% PTFE. Nafion 115 polymer membranes (DuPont) were used to fabricate MEAs. Before being applied to the electrodes, the membranes were pretreated by sequential immersion in boiling solution of 3 wt.% H_2O_2 solution, ultra-pure water, boiling solution of 0.5 mol L^{-1} H_2SO_4, and ultra-pure water, where each step lasted for 1 h. The pretreated Nafion membranes sandwiched between anode and cathode and then the assemblies were hot pressed under a specific load of 100 kg cm^{-2} for 1.5 min at 135 °C.

2.2. Electrochemical measurements

2.2.1. Single fuel cell tests

The electrochemical tests of MEA were carried out by Fuel Cell Testing System (Arbin Instrument Corp.) using the single cell (Electrochemistry Corp.). All of the electrochemical measurements were carried out at 60°C. The 1.5 mol L^{-1} DME solution was fed to the anode side with a flow rate of 3 mL min^{-1}. Pure oxygen was supplied to the cathode side with a flow rate of 200 mL min^{-1} under ambient pressure. The polarization curves and power density curves of the MEA were plotted at intervals of operating time. Each point on the polarization curves and power density curves represented a steady-state performance achieved after about 3 min of continuous operation at a given voltage. The voltage–time curve of the single cell was plotted in a galvanostatic mode with a current density of 30 mA cm^{-2} for 70.5 h. The 70.5 h operation was composed of a 40.5 h operation beginning, and then CV scans of the anode and cathode, and another 30 h operation. In order to maintain the fuel at a stable concentration, the discharge was interrupted at intervals of 5 h, and 1.5 mol L^{-1} fresh DME solution was re-injected. DME solution in reservoir was entirely replaced.

2.2.2. Electrochemical impedance spectra (EIS)

The EIS of the MEA was measured under cell voltage at 0.4 V using an electrochemical analysis instrument (model CHI 604B, Shanghai Chen-Hua Instruments Corp., China) in a frequency range from 1 kHz to 0.01 Hz with 6–12 points per decade. The amplitude of the AC-voltage was 0.005 V.

2.2.3. Cyclic voltammetry

The CV scan was executed by a CHI 604B Electrochemical Analyzer to evaluate the degradation of anode electrochemical active surface (EAS). The anodic EAS at different conditions could be determined through Eq. (1),

$$EAS_H = \frac{Q_H}{[Pt] \times 0.21} \quad (1)$$

where [Pt] denoted Pt loading (mg cm^{-2}) on the electrode, Q_H represented the charge (mC cm^{-2}) for hydrogen desorption, and 0.21 was the required charge (mC cm^{-2}) to oxidize a monolayer of H_2 on bright Pt. During the test, the anode was protected by pure N_2 at a flow rate of 200 mL min^{-1}. Simultaneously, the cathode was fed with humidified H_2 at a flow rate of 200 mL min^{-1} as a dynamic hydrogen electrode (DHE). The CV sweep was performed at a scan rate of 0.01 V s^{-1} between 0.05 and 1.2 V (vs. the cathode). The anodic EAS was determined by calculating the charge for the hydrogen desorption peak [30,31]. The similar CV tests were also employed to detect and eliminate the intermediates from DME electro-oxidation after the 40.5 h operation of the DDFC [18,32]. During the test, the anode was protected by pure N_2 at a flow rate of 200 mL min^{-1}. Simultaneously, the cathode was fed with humidified H_2 at a flow rate of 200 mL min^{-1} as a DHE. The CV sweep was performed at a scan rate of 0.01 V s^{-1} between 0.05 and 1.2 V (vs. the cathode). Another CV scan was carried out to verify the degradation of anode DME oxidation reaction (DOR) activity. 1.5mol L^{-1} DME solution was fed to the anode side with a flow rate of 3 mL min^{-1}. The cathode was fed with humidified N_2 at a flow rate of 200 mL min^{-1} as a DHE [25]. The scan rate was 0.01 V s^{-1} between 0.05 and 1.2 V (vs. the cathode).

Table 1
Voltage decay rate in each operating period during the durability test.

Operating time (h)	Voltage decay rate (mV h^{-1})
0–5	11.4
5–10	11.6
10–15	10.4
15–20	10
20–25	13.2
25–30	15.4
30–35	16.6
35–40	18.8
40–40.5	206
40.5–45.5	17.6
45.5–50.5	18
50.5–55.5	22
55.5–60.5	25.2
60.5–65.5	28.2
65.5–70.5	26

Table 2
Fitting results of EIS results.

Resistances (Ω)	Initial	Aged
R_E	0.26	0.27
$R_{R,C}$	0.07	0.44
R_{CO}	1.0	4.16
$R_{CT,DOR}$	1.2	5.19
$R_{R,A} = (R_{CO}^{-1} + R_{CT,DOR}^{-1})^{-1}$	0.55	2.31
$R_{R,cell} = R_{R,C} + (R_{CO}^{-1} + R_{CT,DOR}^{-1})^{-1}$	0.62	2.75

2.3. Physical measurements

2.3.1. X-ray diffraction (XRD)

XRD analysis of the Pt/C scraped from the initial and aged anodes was carried out with the D/max-RB X-ray diffractometer (made in Japan) using a Cu Ka radiation source at a tube current of 100 mA and a tube voltage of 45 kV, with a scan rate of 4° min^{-1}.

2.3.2. Transmission electron microscopy (TEM)

TEM for the catalyst samples was taken by a Hitachi H-7650 transmission electron microscope. Before taking the electron micrographs, the samples were finely ground and ultrasonically dispersed in isopropyl alcohol, and a drop of the resultant dispersion was deposited and dried on a standard copper grid coated with a polymer film.

2.3.3. Energy dispersive analysis of X-ray (EDAX)

Chemical composition analysis by EDAX was performed with an EDAX Hitachi-S-4700 analyzer associated with a SEM (Hitachi Ltd.,

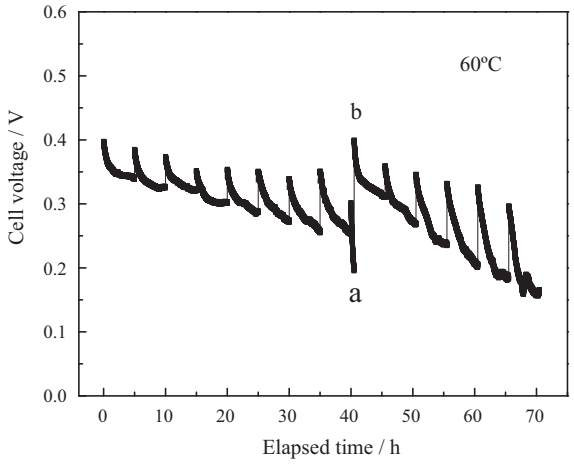

Fig. 1. Voltage-time curve of the single cell discontinuously operated for 70.5 h at a constant current density of 30 mA cm^{-2} at 60 °C. Anode Pt loading: 3.2 mg cm^{-2}; cathode Pt loading: 2.5 mg cm^{-2}. Anodic feed: 1.5 mol L^{-1} DME solution with a flow rate of 3 mL min^{-1}. Cathodic feed: oxygen at ambient pressure with a flow rate of 200 mL min^{-1}. The spikes at a and b were caused by the CV scans of anode and cathode at 40.5 h.

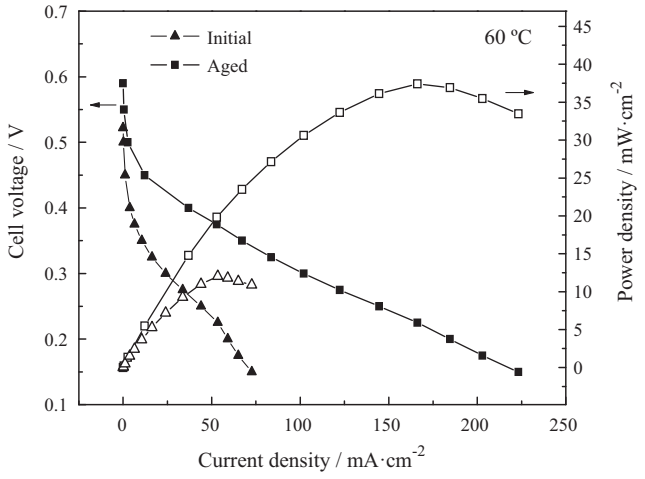

Fig. 2. The polarization curves and the power density curves of DDFC before and after the durability test. Temperature: 60 °C. Anodic feed: 1.5 mol L^{-1} DME solution with a flow rate of 3 mL min^{-1}. Cathode feed: oxygen under ambient pressure with a flow rate of 200 mL min^{-1}.

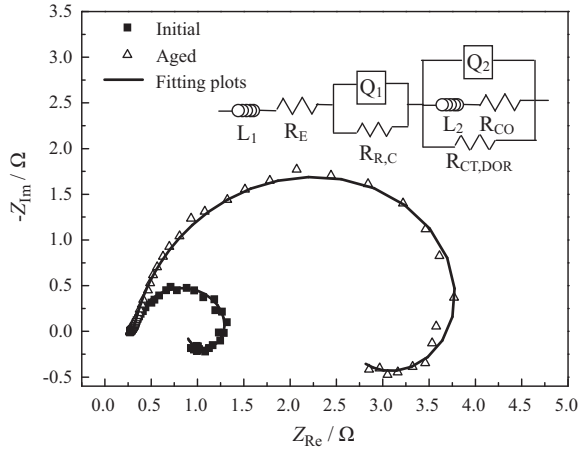

Fig. 3. Nyquist diagrams (dots) of MEA at initial and aged conditions at 0.4 V, and fitting diagrams (lines) based on possible equivalent circuits.

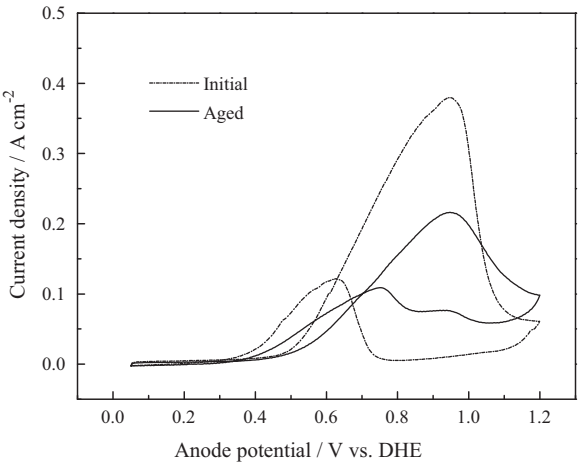

Fig. 4. Anode electro-catalytic activity towards DME oxidation reaction in DDFC.

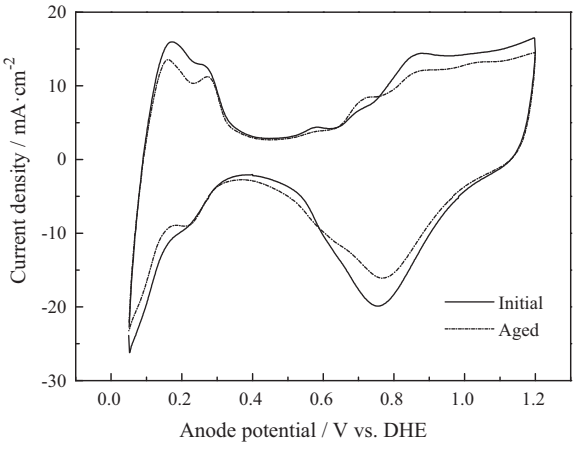

Fig. 5. Cyclic voltammograms of Pt at the initial and aged anode in DDFC, at a scan rate of 0.01 V s^{-1}, in a potential range between 0.05 and 1.2 V vs. DHE.

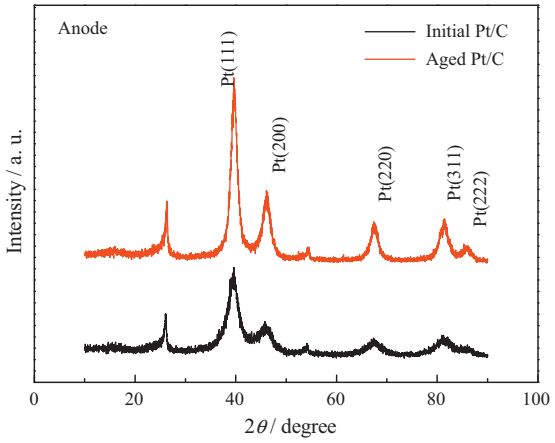

Fig. 6. XRD patterns of anodic catalysts before and after durability test.

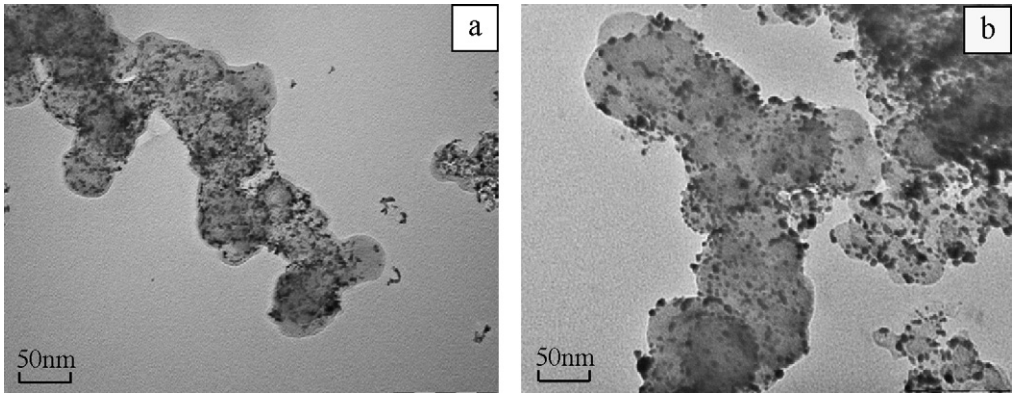

Fig. 7. TEM images of anodic Pt catalyst before and after durability test: (a) initial Pt/C; (b) aged Pt/C.

S-4700). The sample surface was impinged from the normal angle for 100 s by the incident electron beam with energies ranging from 3 to 30 keV.

3. Results and discussion

The voltage–time curve at a constant current density of 30 mA cm^{-2} is shown in Fig. 1. It is observed that, during each continuous discharge process, the cell voltage decreases with time but could be partially recovered after every interruption. The possible reasons are the replenishment of DME fuel and water removal at the cathode during the stop of cell operation. During the whole test process, the cell voltage decreases with time. The voltage decay rate in each operating period is listed in Table 1. The decay rate is calculated by dividing voltage loss during each operating period by time elapsed in each operating period. Before operating time of 40 h, the voltage decay rate increases slightly. During the 40–40.5 h period, the voltage decay rate increases dramatically. The sudden change of the decay rate might imply great changes in the health of MEA. After the 40.5 h operation, CV scans are carried out on both anode and cathode to detect and purge the absorbed DME oxidation intermediates. After the CV scans, the durability test is going on. The cell voltage increases and the voltage decay rate decreases after the CV scans. It indicates that absorbed DME oxidation intermediates species on electrodes have been oxidized by CV scans and the effective Pt active sites are increased. The electrochemical reactions activities are partially recovered by CV scans.

The cell performances before and after 70.5 h durability test are compared by polarization and power density curves at a temperature of 60 °C as shown in Fig. 2. The maximum power density drops dramatically from an initial value of 37 mW cm^{-2} to 12 mW cm^{-2}. The current densities and potentials at which the maximum power density occurs also decrease after the durability test. In low current density region where the overall cell reaction is governed by electrochemical process, the aged MEA suffers from an obvious potential loss due to the faded electrochemical activity. DDFC performance degradation is closely correlated with the degradation of the catalyst layer. On the other hand, open circuit potential of DDFC decreases from 0.59 V to 0.52 V. The open circuit potential loss of DDFC may be due to increased DME crossover.

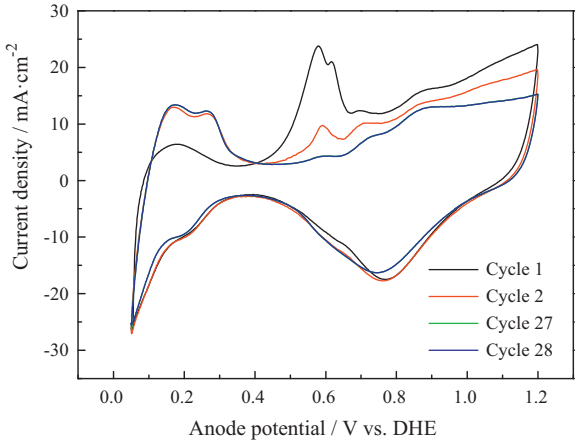

Fig. 8. Cyclic voltammograms of anode after 40.5 h operation, at a scan rate of 0.01 V s^{-1}, in a potential range between 0.05 and 1.2 V vs. DHE.

The EIS of the initial and aged MEA are carried out at a cell voltage of 0.4 V. The Nyquist diagrams are illustrated in Fig. 3. Moreover, the fitting results of the resistance elements are listed in Table 2. The ohmic resistance (R_E) slightly increases from 0.26 Ω to 0.27 Ω and it makes little contribution to DDFC performance deterioration. As seen in Fig. 2, DDFC operates in low current region at a cell voltage of 0.4 V. In low current region, the overall cell reaction is dominated by electrochemical process, so mass transport process can be ignored. Therefore, the Nyquist diagrams correspond to the oxygen reduction reaction and the DME oxidation reaction [28]. The Faraday impedance of the cathode and the anode can be expressed as Eqs. (2) and (3). As reported previously [33,34], the inductance at low frequency region is presumed to result from the slow relaxation of the adsorbed CO at the anode side. A widely used equivalent circuit [22] in Fig. 3, involving the ohmic resistance, O_2 reduction, DME dehydrogenation and intermediate oxidation process, is suggested to describe the DDFC total cell reaction. The cathode reaction resistance ($R_{R,C}$) increases from 0.07 Ω to 0.44 Ω. Cathode degradation also contributes to DDFC performance deterioration. $R_{CT,DOR}$ and R_{CO} symbolize the charge transfer resistances of elementary reactions corresponding to DME and CO_{ADS}, respectively. The increase in $R_{CT,DOR}$ means that DME dehydrogenation becomes more difficult. The increase in R_{CO} means that poisoning of the Pt becomes more serious after durability test. The total cell reaction resistance ($R_{R,cell}$) increases from 0.62 Ω to 2.75 Ω. The anode reaction resistance ($R_{R,A}$) increases from 0.55 Ω to 2.31 Ω. The DDFC performance degradation can largely be attributed to the increase in the anode reaction resistance rather than that of the cathode.

$$\frac{1}{Z_{f,C}} = \frac{1}{R_{R,C}} + Y_0\omega^n \cos\left(\frac{n\pi}{2}\right) + jY_0\omega^n \sin\left(\frac{n\pi}{2}\right) \quad (2)$$

$$\frac{1}{Z_{f,A}} = \frac{1}{R_{CT,DOR}} + \frac{1}{R_{CO} + j\omega L} + Y_0\omega^n \cos\left(\frac{n\pi}{2}\right) + jY_0\omega^n \sin\left(\frac{n\pi}{2}\right) \quad (3)$$

Fig. 4 shows the CV curves of DME electrooxidation on the initial and aged anode at a scan rate of 0.01 V s^{-1} at 60 °C. CV curves of

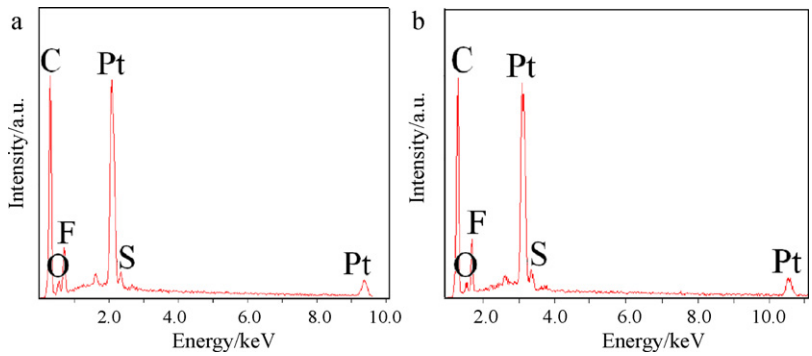

Fig. 9. EDAX patterns of surface species in the initial and aged anodic catalyst layer: (a) initial Pt/C; (b) aged Pt/C.

DME electrooxidation in Fig. 4 characterize electrochemical activity of anode. The lower onset potential and the higher peak current density in CV curves are, the higher the anode activity is. It can be observed from Fig. 4 that the onset potential and peak potential of DME electrooxidation are almost the same after the durability test, about 0.48 V and 0.92 V (vs. DHE), respectively. However, there is obvious decrease in the peak current densities (from 0.38 A cm^{-2} to 0.22 A cm^{-2}) of DME electrooxidation reactions. Fig. 4 clearly shows the performance of the anode drops dramatically after durability test, which result in anode reaction resistance increase in Table 2.

Fig. 5 presents the degradation of the anodic EAS. The H_2 desorption peaks provide the information of the electrochemical active surface of Pt. The EAS decreases from 350 to 288 cm^2 mg^{-1} Pt after 70.5 h operation. It indicates that the 'triple-phase boundaries' where the electrolyte, reaction materials, and electrically connected catalyst particles contact together in anode decrease after the durability tests. The aging of anodic catalyst would be one of the important reasons for the performance decay of DDFC anode.

XRD patterns of anode Pt/C catalyst before and after durability test are shown in Fig. 6. The first diffraction peaks for anode Pt/C catalyst at 2θ about 26° can be attributed to the hexagonal graphite structures (0 0 2) of the carbon black support. The Pt has a face-centered cubic (fcc) structure showing the major peaks of Pt (1 1 1), Pt (2 0 0), Pt (2 2 0), Pt (3 1 1), and so on. The Pt (2 2 0) peak is selected to calculate the mean particle size of Pt catalysts before and after the durability test according to Debye–Scherrer formula because it is isolated from the diffraction peaks of carbon support [35]. The particle size of anodic catalyst grows from an initial value of 3.0 nm to 5.5 nm. The high sintering rate of the anodic catalyst may be due to DME highly aggressive towards electrocatalyst. The effect of DME on the aging of anodic catalyst is critical in our work. Furthermore, small Pt particles are unstable due to agglomeration in an electrochemical environment during operation.

Fig. 7 presents the TEM images of anode Pt/C catalyst before and after durability test. It can be seen from Fig. 7(a) that the size of Pt nanoparticles before durability test is small, and their dispersion on carbon support is very even without agglomeration. After the durability test, the catalyst particles grow up evidently, which is consistent with the above XRD results. The growth of the Pt particles resulting in anodic EAS degradation, which cause the increase in anode reaction resistance and decrease in the peak current densities of DME electrooxidation reactions. Pt particles growth must be the main cause of the anode catalyst failure.

Fig. 8 shows the CV scans of anode after 40.5 h operation. After the CV scans, the performance of DDFC is dramatically enhanced and the voltage decay rate is decreased. All these changes are likely to be caused by the oxidation of adsorbed DME oxidation intermediates species that accumulate on the anode Pt catalyst surface. With an increasing cycling number, the oxidation peak of the adsorbed species gradually decreases. Simultaneously, the H_2 desorption peak recovers. The CV profiles reach a steady state with the 27th cycle, and no further changes are observed from cycle 27 to cycle 28, which indicates that the absorbed intermediates have been fully purged. The poisoning of catalysts can debase the long-term performance of DDFC. The decrease in effective Pt active sites deriving from poisoning of Pt must be another cause of dramatically increase in anode reaction resistance and decrease in the peak current densities of DME electrooxidation reactions. Furthermore, DME dehydrogenation on Pt surface needs at least three contiguous Pt active sites [12]. The growth and poisoning of the Pt particles result in decrease in contiguous Pt sites, which lead to increase in $R_{CT,DOR}$.

The EDAX results of the initial and aged anodic catalyst layer are presented in Fig. 9. The Pt contents are 33.1 and 33.9 wt.% in initial and aged anodic catalyst layers, respectively, which are similar to the theoretical values. The theoretical values of Pt content in catalyst layer is 32 wt.%, which is the product of theoretical Pt content in anode catalyst (40 wt%) and catalyst content in anode catalyst layer (80 wt%). It is revealed that the Pt metal in anodic catalyst does not evidently dissolve during operation. The decay of anode performance might not be correlated with the dissolution of Pt metal in anode catalyst.

4. Conclusions

The durability test of a DDFC is carried out at a constant current density of 30 mA cm^{-2} for 70.5 h discontinuous operation under ambient pressure and at a cell temperature of 60 °C. The maximum power density of DDFC decreases from 37.4 mW cm^{-2} to 12.0 mW cm^{-2}. The anode EAS reduces from 350 to 288 cm^2 mg^{-1} Pt after 70.5 h operation. The anode degradation is mainly caused by the growth of Pt particles and the poisoning of catalyst by absorbed DME oxidation intermediates. The dissolution of anode Pt catalyst is not observed during the durability test, and hence Pt catalyst dissolution does not affect the durability of DDFC in this study.

Acknowledgement

This work is financially supported by National Natural Science Foundation of China (Grant No. 50872027, 21106024, and 21173062), Ministry of Science and Technology of China (863 program Grant No. 2009AA05Z111), and Fundamental Research Funds for the Central Universities (HIT.ICRST.2010006).

References

[1] T.S. Zhao, W.W. Yang, R. Chen, Q.X. Wu, J. Power Sources 195 (2010) 3451–3462.
[2] Y.Y. Shao, J. Liu, Y. Wang, Y.H. Lin, J. Mater. Chem. 19 (2009) 46–59.
[3] S. Zhang, Y.Y. Shao, G.P. Yin, Y.H. Lin, Angew. Chem. Int. Ed. 49 (2010) 2211–2214.

[4] Y.Y. Chu, Z.B. Wang, Z.Z. Jiang, D.M. Gu, G.P. Yin, Adv. Mater. 23 (2011) 3100–3104.
[5] S. Ueda, M. Eguchi, K. Uno, Y. Tsutsumi, N. Ogawa, Solid State Ionics 177 (2006) 2175–2178.
[6] Y. Liu, S. Mitsushima, K.-I. Ota, N. Kamiya, Electrochim. Acta 51 (2006) 6503–6509.
[7] J.H. Yu, H.G. Choi, S.M. Cho, Electrochem. Commun. 7 (2005) 1385–1388.
[8] Y. Liu, M. Muraoka, S. Mitsushima, K.I. Ota, I. Kamiya, Electrochim. Acta 52 (2007) 5781–5788.
[9] G. Kerangueven, C. Coutanceau, E. Sibert, J.M. Leger, C. Lamy, J. Power Sources 157 (2006) 318–324.
[10] K. Xu, S.J. Lao, H.Y. Qin, B.H. Liu, Z.P. Li, J. Power Sources 195 (2010) 5606–5909.
[11] J.R. Ferrell, M.C. Kuo, A.M. Herring, J. Power Sources 195 (2010) 39–45.
[12] L.L. Lu, G.P. Yin, Z.B. Wang, K.D. Cai, Y.Z. Gao, Catal. Commun. 10 (2009) 971–974.
[13] Y.J. Tong, L.L. Lu, Y. Zhang, Y.Z. Gao, G.P. Yin, M. Osawa, Y. Shen, J. Phys. Chem. C 111 (2007) 18836–18838.
[14] Y. Zhang, L.L. Lu, Y.J. Tong, M. Osawa, S. Ye, Electrochim. Acta 53 (2008) 6093–6103.
[15] L.H. Xing, Y.Z. Gao, Z.B. Wang, C.Y. Du, G.P. Yin, Int. J. Hydrogen Energy 36 (2011) 11102–11107.
[16] L.H. Xing, Z.B. Wang, C.Y. Du, G.P. Yin, Int. J. Energy Res., doi:10.1002/er.1857.
[17] L.H. Jiang, G.Q. Sun, S.L. Wang, G.X. Wang, Q. Xin, Z.H. Zhou, B. Zhou, Electrochem. Commun. 7 (2005) 663–668.
[18] Y. Zhai, G. Bender, S. Dorn, R. Rocheleau, J. Electrochem. Soc. 157 (2010) B20–B26.
[19] N. Zamel, X.G. Li, Int. J. Hydrogen Energy 33 (2008) 1335–1344.
[20] J. Prabhuram, N.N. Krishnan, B. Choi, T.H. Lim, H.Y. Ha, S.K. Kim, Int. J. Hydrogen Energy 35 (2010) 6924–6933.
[21] W.M. Chen, G.Q. Sun, J.S. Guo, X.S. Zhao, S.Y. Yan, J. Tian, S.H. Tang, Z.H. Zhou, Q. Xin, Electrochim. Acta 51 (2006) 2391–2399.
[22] P. Liu, G.P. Yin, K.D. Cai, Electrochim. Acta 54 (2009) 6178–6183.
[23] W.G. Schmittinger, A. Vahidi, J. Power Sources 180 (2008) 1–4.
[24] Z.B. Wang, Y.Y. Shao, P.J. Zuo, X.P. Wang, G.P. Yin, J. Power Sources 185 (2008) 1066–1072.
[25] H.C. Cha, C.Y. Chen, J.Y. Shiu, J. Power Sources 192 (2009) 451–456.
[26] Y.Y. Shao, S. Zhang, C.M. Wang, Z.M. Nie, J. Liu, Y. Wang, Y.H. Lin, J. Power Sources 195 (2010) 4600–4605.
[27] Z.B. Wang, X.P. Wang, P.J. Zuo, B.Q. Yang, G.P. Yin, X.P. Feng, J. Power Sources 181 (2008) 93–100.
[28] M.K. Jeon, J.Y. Won, K.S. Oh, K.R. Lee, S.I. Woo, Electrochim. Acta 53 (2007) 447–452.
[29] J.G. Liu, Z.H. Zhou, X.S. Zhao, Q. Xin, G.Q. Sun, B.L. Yi, Phys. Chem. Chem. Phys. 6 (2004) 134–137.
[30] S. Zhang, Y.Y. Shao, H.G. Liao, M.H. Engelhard, G.P. Yin, Y.H. Lin, ACS Nano 5 (2011) 1785–1791.
[31] F. Xie, C. Chen, H. Meng, P.K. Shen, Fuel Cells 07 (2007) 319–322.
[32] D.J. Yang, J.X. Ma, L. Xu, M.Z. Wu, H.J. Wang, Electrochim. Acta 51 (2006) 4039–4044.
[33] J.T. Müller, P.M. Urban, W.F. Holderich, J. Power Sources 84 (1999) 157–160.
[34] S. Tominaka, N. Akiyama, T. Momma, T. Osaka, J. Electrochem. Soc. 154 (2007) B902–B909.
[35] S. Zhang, Y.Y. Shao, G.P. Yin, Y.H. Lin, J. Mater. Chem. 20 (2010) 2826–2830.